Fluid Dynamics and Co-located Conferences
June 24-27, 2013, San Diego, CA
21st AIAA Computational Fluid Dynamics Conference

High-order schemes for cylindrical/spherical geometries with cylindrical/spherical symmetry

Sheng Wang* and Eric Johnsen†
University of Michigan, Ann Arbor, MI 48109, USA

In this paper, we implement finite volume Weighted Essentially Non-Oscillatory (WENO) schemes in both cylindrical and spherical coordinate systems for the Euler equations with cylindrical or spherical symmetry. We analyze three different spatial discretizations: one that is shown to be high-order accurate but not conservative, one conservative but not high-order accurate, and one both high-order accurate and conservative. For cylindrical and spherical coordinates, we present convergence results for the advection equation and the Euler equations with an acoustics problem. We then use the Sod shock tube and the Sedov point-blast problems in spherical coordinates coordinates to verify our analysis and implementations.

I. Introduction

Across a variety of disciplines in science and engineering, physical systems that exhibit either cylindrical or spherical symmetry are often encountered. Examples of interest include astrophysics (e.g., supernova collapse), nuclear explosions, inertial confinement fusion (ICF) and naval engineering (e.g., cavitation-bubble dynamics and collapse), amongst others. A natural approach to solving these problems numerically is to discretize the governing partial differential equations in cylindrical/spherical coordinates. Historically, the first such numerical studies were conducted by Von Neumann and Richtmyer[17] in the 1940s for nuclear explosions. To treat the discontinuities in a stable fashion, they introduced artificial dissipation terms to the Euler equations. While this method correctly captures the position of shocks and satisfies the Rankine-Hugoniot equations, discontinuities in the numerical solution are smeared out due to the excessive dissipation.

The collapse of cavitation bubbles and supernovae, and ICF share similarities in that they are all, under ideal circumstances, spherically symmetric converging flows that involve material interfaces, accelerations and shocks. Such flow are rarely ideal, insofar as they are prone to interfacial instabilities due to accelerations (Rayleigh-Taylor[16]), shocks (Richtmyer-Meshkov[2]), or geometry (Bell-Plesset[3,4]). For large three-dimensional perturbations, cylindrical/spherical coordinates may not be advantageous. However, in a number of problems such as sonoluminescence,[5] the spherical symmetry assumption is remarkably valid. Modeling the bubble motion with spherical symmetry can greatly reduce the computational cost. Akhatov, et al.[1] used a first-order Godunov scheme to simulate the fluid behavior outside of bubble and the Rayleigh-Plesset equation for the bubble dynamics. This approach is based on spherical symmetry assumption and not able to capture the shock wave inside of single bubble.

Several recent studies in cylindrical and spherical coordinates have focused on the Lagrangian form. The compressible Euler equations in cylindrical or spherical geometry have been studied by Maire,[14] using a cell-centered Lagrangian scheme, which ensures conservation of momentum and energy. These equations were also studied by Omang et al.[15] using Smoothed Particle Hydrodynamics (SPH), though SPH methods are generally not high-order accurate. On the other hand, solving the equations in Eulerian form is not trivial, especially when trying to ensure conservation and high-order accuracy. Li[13] attempted to implement Eulerian finite difference and finite volume weighted essentially non-oscillatory (WENO) schemes[9] in cylindrical and spherical grid, but did not achieve acceptable results. Johnsen & Colonius[10,11] used cylindrical coordinates with azimuthal symmetry to directly simulate the axisymmetric collapse of initially spherical gas bubbles in shock-wave lithotripsy, by solving the Euler equations inside and outside the bubble.

*Undergraduate Student, Nuclear Engineering Department, AIAA Student Member.
†Assistant Professor, Mechanical Engineering Department, AIAA Member.

In this paper, we investigate three different spatial discretizations in cylindrical/spherical coordinates with cylindrical/spherical symmetry using finite volume WENO. The governing equations are stated in Section II and the spatial discretizations are presented in Section III. In Section IV, we test the different discretizations on smooth problems (scalar advection equation, acoustics problem for the Euler equations) for convergence, and with shock-dominated problems (Sod shock tube and Sedov point blast problems) for conservation. The last section summarizes the present work and provides a future outlook.

II. Governing equations

The Euler equations describe the physics of inviscid, compressible flow. In cylindrical/spherical coordinates with cylindrical/spherical symmetry these equations can be written in divergence form:

$$(\rho)_t + \frac{1}{r^\alpha}\left(r^\alpha \rho u\right)_r = 0, \tag{1a}$$

$$(\rho u)_t + \frac{1}{r^\alpha}\left(r^\alpha \rho u^2\right)_r + p_r = 0, \tag{1b}$$

$$(E)_t + \frac{1}{r^\alpha}\left(r^\alpha \left(E+p\right) u\right)_r = 0, \tag{1c}$$

where t is time, r is the radial coordinate, p is the pressure, ρ is the density, E is the total energy, and α is a geometric parameter, which is 0, 1, or 2 for Cartesian, cylindrical, or spherical coordinates, respectively. Subscripts denote derivatives. For an ideal gas, the equation of state to close this system can be written:

$$p = (\gamma - 1)\,\varepsilon, \tag{2}$$

where $\varepsilon = E - \rho u^2/2$ is the internal energy, and γ is the specific heats ratio. Here, diffusion effects are neglected.

III. Spatial discretization

In this section, we analyze three different discretizations of the Euler Eqs.(1) in cylindrical/spherical coordinates, based on different forms of the convective terms. While the discretized form of the Euler equations in Cartesian coordinates is generally designed to conserve mass, momentum and energy, the conservation condition does not necessarily hold in cylindrical or spherical coordinates, depending on the numerical treatment of the equations. Here, finite volume refers to the WENO approach that is followed: first a reconstruction of the appropriate variables, then application of a Riemann solver to obtain the appropriate cell-edge value.

Method One

The first spatial discretization, labelled *Method One* here, can be found in Toro.[18] The mass, momentum, and energy equations are written in semi-discrete form:

$$\frac{\mathrm{d}\rho_i}{\mathrm{d}t} = -\frac{(\rho u)_{i+1/2} - (\rho u)_{i-1/2}}{\Delta r} - \frac{\alpha}{r_i}\left(\rho u\right)_i, \tag{3a}$$

$$\frac{\mathrm{d}(\rho u)_i}{\mathrm{d}t} = -\frac{(\rho u + p)_{i+1/2} - (\rho u + p)_{i-1/2}}{\Delta r} - \frac{\alpha}{r_i}\left(\rho u^2\right)_i, \tag{3b}$$

$$\frac{\mathrm{d}E_i}{\mathrm{d}t} = -\frac{((E+p)u)_{i+1/2} - ((E+p)u)_{i-1/2}}{\Delta r} - \frac{\alpha}{r_i}\left(u(E+p)\right)_i, \tag{3c}$$

where Δr is the linear radial cell width. Here,

$$\rho_i = \frac{1}{\Delta V}\int_{I_i} \rho dV, \tag{4}$$

where I_i denotes cell i, and $dV \sim r^\alpha dr$.

In Method One, physical variables expected to be conserved are not necessarily conserved numerically because this approach is derived from differential form of the equations, rather than integral form. High-order accuracy may be achieved with this method.

Method Two

The second discretization, Method Two, is based on the integral form of the equation. The mass, momentum, and energy equations are written in semi-discrete form:

$$\frac{\mathrm{d}\rho_i}{\mathrm{d}t} = -\frac{r^\alpha_{i+1/2}(\rho u)_{i+1/2} - r^\alpha_{i-1/2}(\rho u)_{i-1/2}}{\Delta V}, \tag{5a}$$

$$\frac{\mathrm{d}(\rho u)_i}{\mathrm{d}t} = -\frac{r^\alpha_{i+1/2}(\rho u^2 + p)_{i+1/2} - r^\alpha_{i-1/2}(\rho u^2 + p)_{i-1/2}}{\Delta V} + S(r), \tag{5b}$$

$$\frac{\mathrm{d}E_i}{\mathrm{d}t} = -\frac{r^\alpha_{i+1/2}((E+p)u)_{i+1/2} - r^\alpha_{i-1/2}((E+p)u)_{i-1/2}}{\Delta V}, \tag{5c}$$

where $\Delta V = \frac{1}{1+\alpha}(r^{\alpha+1}_{i+1/2} - r^{\alpha+1}_{i-1/2})$ and $S(r)$ is the source term in momentum equation, which depending on the chosen coordinate system can be expressed as:

$$S(r) = \frac{r^\alpha_{i+1/2}p_{i+1/2} - r^\alpha_{i-1/2}p_{i-1/2}}{\Delta V} - \frac{p_{i+1/2} - p_{i-1/2}}{\Delta r}. \tag{6}$$

Depending on the reconstruction procedure, the first term may cancel the corresponding term in the momentum equation. In Method One, setting the geometrical source term to an average $((\cdot)_{i+1/2} + (\cdot)_{i-1/2})/2$ in an attempt to preserve conservation yields Method Two. Again,

$$\rho_i = \frac{1}{\Delta V}\int_{I_i} \rho dV. \tag{7}$$

With this approach, the relevant physical variables are expected to be conserved. However, high-order accuracy may be difficult to achieve. This latter point can be readily understood by subtracting Method Two from Method One, which is high-order accurate.

Method Three

The third spatial discretization, Method Three, is inspired by solutions to acoustics problems in cylindrical and spherical coordinates. Multiplying Eqs. (1) by r^α, the mass, momentum, and energy equations are written in semi-discrete form:

$$\frac{\mathrm{d}(r^\alpha\rho)_i}{\mathrm{d}t} = -\frac{(r^\alpha\rho u)_{i+1/2} - (r^\alpha\rho u)_{i-1/2}}{\Delta r}, \tag{8a}$$

$$\frac{\mathrm{d}(r^\alpha\rho u)_i}{\mathrm{d}t} = -\frac{(r^\alpha(\rho u^2 + p))_{i+1/2} - (r^\alpha(\rho u^2 + p))_{i-1/2}}{\Delta r} + \alpha(pr^{\alpha-1})_i, \tag{8b}$$

$$\frac{\mathrm{d}(r^\alpha E)_i}{\mathrm{d}t} = -\frac{(r^\alpha(E+p)u)_{i+1/2} - (r^\alpha(E+p)u)_{i-1/2}}{\Delta r}. \tag{8c}$$

Here,

$$(r^\alpha\rho)_i = \frac{1}{\Delta r}\int_{I_i} \rho r^\alpha dr. \tag{9}$$

With this approach, the conserved variables are ($r^\alpha\rho$, $r^\alpha\rho u$, $r^\alpha E$). This approach is expected to be both conservative and high-order accurate.

IV. Numerical results

In this section, we apply the three discretizations introduced in the previous section in four test cases using fifth-order WENO in characteristic space with Local Lax-Friedrichs, and fourth-order accurate explicit Runge-Kutta with a Courant number of 0.5 for time marching. First, we use two smooth problems (scalar advection and acoustics for the Euler equations) to demonstrate the convergence properties of each method for the interior solution, with no regards for boundary schemes. Next, we test conservation with two shock-dominated problems (Sod shock tube and Sedov point blast problems).

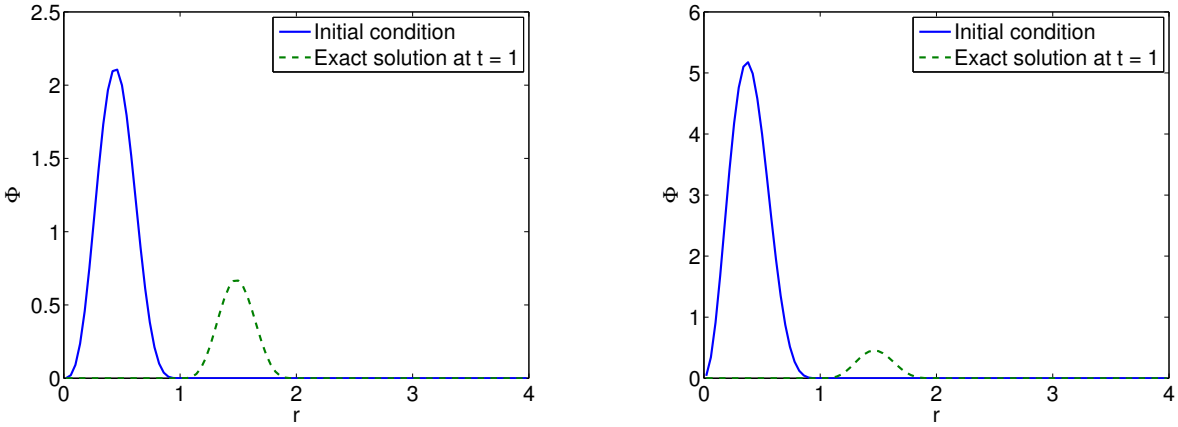

(a) Cylindrical, $\alpha = 1$ (b) Spherical, $\alpha = 2$

Figure 1. Initial conditions and exact solution after $t = 1$ for the advection equation.

1. *Scalar advection problem*

Before considering nonlinear systems, the scalar advection equation is investigated. The advection equation in cylindrical and spherical coordinates with symmetry is written:

$$(\phi)_t + \frac{c_0}{r^\alpha}\left(r^\alpha \phi\right)_r = 0, \tag{10}$$

where ϕ is a scalar field, c_0 is the (constant and known) wave speed. Here, $c_0 = 1$. The initial conditions are

$$\phi(r,0) = \begin{cases} \frac{sin^4(\pi r)}{r^\alpha}, & \text{if } 0 \le r \le 1, \\ 0, & \text{if } r > 1. \end{cases} \tag{11}$$

For this problem, the exact solution at time $t = 1$ is

$$\phi(r,t) = \begin{cases} \frac{sin^4(\pi(r-c_0 t))}{r^\alpha}, & \text{if } c_0 t \le r \le c_0 t + 1, \\ 0, & \text{otherwise.} \end{cases} \tag{12}$$

The initial conditions and exact solution at $t = 1$ are shown in Fig. 1. Nearly identical set-ups are used for the cylindrical and spherical cases, the only difference being the geometrical parameter: $\alpha = 1$ for cylindrical problems, and $\alpha = 2$ for spherical problems.

The goal is to determine the convergence properties of each scheme, independently of boundary schemes. The problem set-up is specifically chosen to prevent any boundary effects. Here, we show only the convergence analysis results for cylindrical coordinates, as the convergence rate is similar for the spherical case. Grids with $N = 21, 41, 81, 161, 321, 641$ are considered with constant Δr, and the exact solution is used to evaluate the error of each solution. Fig. 2 shows the L_2 error norm to verify the order of accuracy. Methods One and Three both achieve fifth-order accuracy, while Method Two is only second-order accurate, as expected from the discussion in the previous section.

2. *Euler equations: acoustics problem*

Since a smooth problem is needed to verify convergence with the Euler equations, the acoustics problem from Johnsen & Colonius[6] is adapted to spherical coordinates. The initial conditions are

$$\rho(r,0) = 1 + \varepsilon f(r), \tag{13a}$$
$$u(r,0) = 0, \tag{13b}$$
$$p(r,0) = 1/\gamma + \varepsilon f(r), \tag{13c}$$
$$\tag{13d}$$

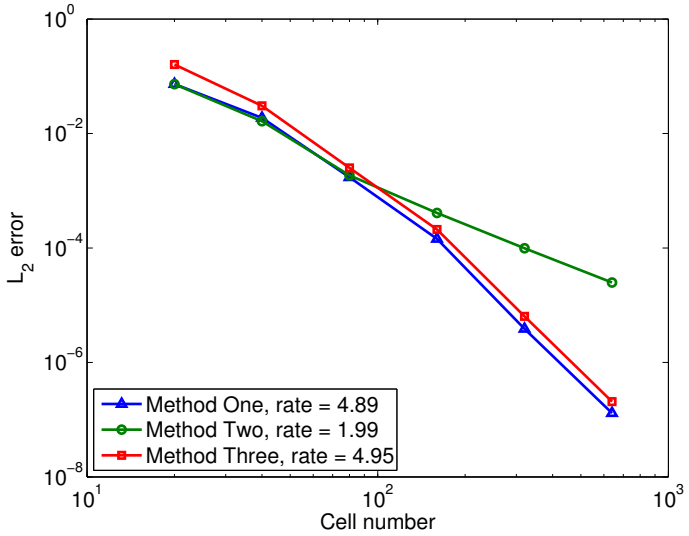

Figure 2. L_2 **error norm for all three discretizations for the advection equation.**

with perturbation

$$f(r) = \begin{cases} \frac{sin^4(\pi r)}{r}, & \text{if } 0.4 \leq r \leq 0.6, \\ 0, & \text{otherwise.} \end{cases} \tag{14}$$

For a sufficiently small ε (here 10^{-4}), the solution remains very smooth. In this problem, the initial perturbation splits into two acoustic waves traveling in opposite directions. To prevent the singularity at the origin and boundary effects, the solution is not computed there. This is not a problem, since the wave has not yet reached that point by the final time. Again, grids with $N = 21$, 41, 81, 161, 321 and 641 are used with constant Δr. Although an exact solution to order ε^2 is known, the result on the finest grid is used as the reference to evaluate the error.

Fig. 3 shows the L_2 error in density for this problem. The results show that Methods One and Three remain high-order and in fact fall on top of each other, although the rate now is reduced to fourth order; it should be noted that in Johnsen & Colonius[6] fifth-order accuracy is not always readily achieved. For Method Two, the rate is close to second order, as expected.

3. Sod shock tube

In this subsection, we consider the Sod shock tube problem[12] in spherical coordinate. The initial condition for the Sod's problem is

$$\begin{pmatrix} \rho \\ u \\ p \end{pmatrix}_L = \begin{pmatrix} 1 \\ 0 \\ 1 \end{pmatrix}, \qquad \begin{pmatrix} \rho \\ u \\ p \end{pmatrix}_R = \begin{pmatrix} 0.125 \\ 0 \\ 0.1 \end{pmatrix}. \tag{15}$$

The domain size is 1 and 100 equally spaced grid points are used. The location of the "diaphragm" separating the left and right states is $r = 0.5$. Non-reflecting boundary conditions are used at the origin and outlet; since no wave reaches the boundaries over the duration of the simulation (final time: $t_{final} = 0.2$), the boundary scheme is irrelevant.

Fig. 4 shows density, velocity, pressure and internal energy profiles for this problem at the final time. On this grid, all three methods produce similar profiles. However, the residuals of the total mass yield different results, as observed in Fig. 5. While Methods Two and Three are conservative to round-off level, Method One is not discretely conservative, as expected. Differences in shock position due to lack of conservation are not clear in this case.

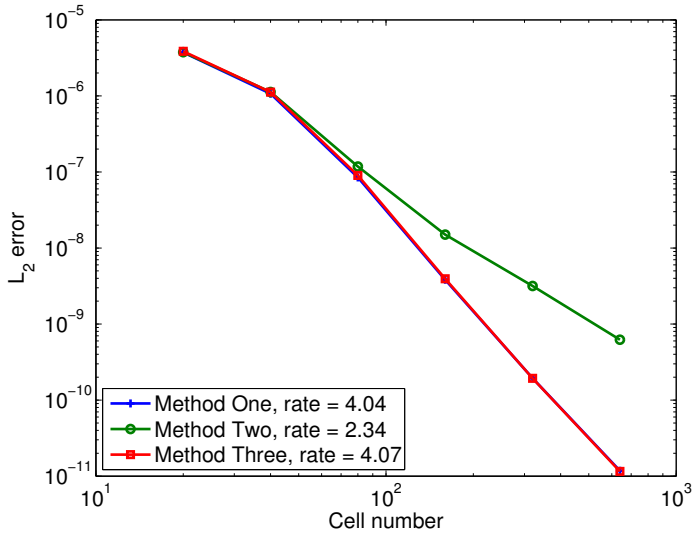

Figure 3. L_2 **error norm for each discretization when solving the Euler equations. Results for Methods One and Three fall on top of each other on this scale.**

4. Sedov point-blast

Finally, we consider the Sedov point-blast problem in spherical coordinates. The problem starts from a delta-function initial pressure perturbation at the center of uniform medium. Following the set-up of Fryxell et al.[7] the initial conditions are

$$\begin{pmatrix} \rho \\ u \\ p \end{pmatrix} = \begin{pmatrix} 1 \\ 0 \\ 1 \end{pmatrix}, \tag{16}$$

except for a few computational cells around the origin, whose pressure is

$$p_0^{'} = \frac{3(\gamma-1)\varepsilon}{(\alpha+1)\pi\delta r^{\alpha}}. \tag{17}$$

Here, $\varepsilon = 1$ is the dimensionless energy. The domain size is 1, and $N = 100$ with uniform spacing. We choose a constant δr to be three times as large as the cell size for $N = 100$. Reflecting boundary conditions[8] are used along the centerline, and non-reflecting conditions are applied at the outlet. Due to the reflecting boundary condition at the center, the high pressure region is made up of 6 cells, i.e., 3 ghost cells and 3 cells in the interior. The solution is plotted at $t = 0.2$.

Density, velocity, pressure and internal energy profiles are shown in Fig. 6. The density profile and mass residual for different grid size are potted in Fig. 7. The difference in shock location is striking for this problem. Method One is non-conservative and thus produces an incorrect shock speed and thus location; it appears to converge to the correct location with grid refinement. This result is confirmed by considering the mass residual. For this problem, Method Three proved to be unstable at the present Courant number due to the boundary scheme.

V. Conclusion

We analyzed three different spatial discretizations in cylindrical/spherical coordinates for the Euler equations using finite volume WENO. In particular, high-order accuracy and conservation were evaluated. Only one of the methods achieved high-order accuracy and was conservative, but it could not handle the Sedov problem at the present CFL. The other methods are either conservative or high-order accurate, but never both.

Current work is underway to extend the analysis and implementations to finite difference and discontinuous Galerkin finite element methods and to incorporate diffusive effects. Reflecting boundary conditions

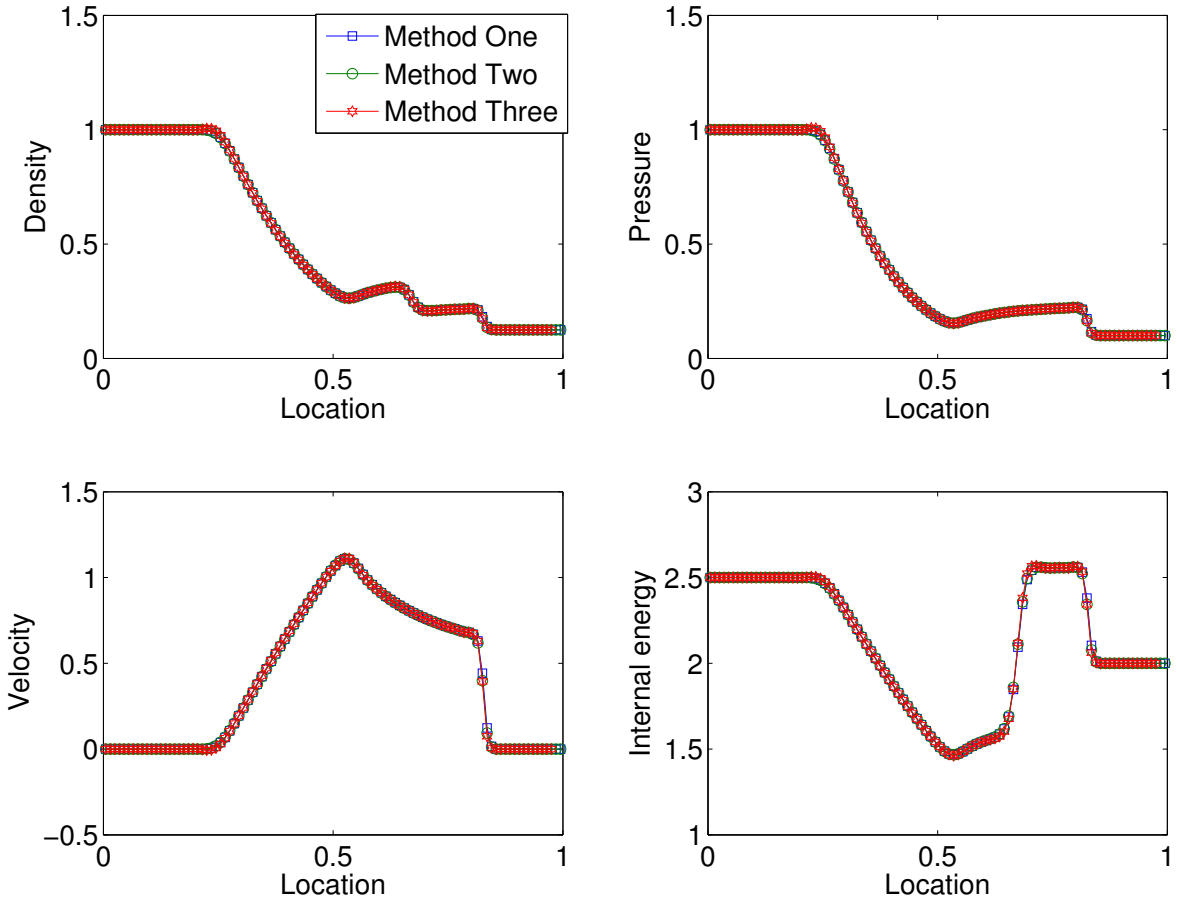

Figure 4. Profiles at $t = 0.2$ for the Sod problem with 100 points.

are not trivial in terms of both high-order accuracy and conservation, and will be investigated subsequently. This approach will form the basis for simulations of cavitation-bubble dynamics and collapse in the context of cavitation erosion.

Acknowledgments

This work was supported in part by ONR grant N00014-12-1-0751 under Dr. Ki-Han Kim.

References

[1]Akhatov, I., Lindau,O., Topolnikov, A., Mettin, R., Vakhitova, N., Lauterborn, W., 2001. Collapse and rebound of a laser-induced cavitation bubble, Phys. Fluids. 13, 2805–2819.

[2]Brouillette, M., 2002. The Richtmyer-Meshkov instability, Annu. Rev. Fluid Mech. 34 445–468.

[3]Bell, G. I., 1951. Taylor instability on cylinders and spheres in the small amplitude approximation, Los Alamos Scientific Laboratory, Los Alamos, NM, Report LA-1321.

[4]Plesset, M. S., and Mitchell, T. M., 1956. On the stability of the spherical shape of a vapour cavity in a liquid, Q. Appl. Math. 13, 419–430.

[5]Barber, B.P., Hiller, R. A., Lofstedt, R., Putterman, S. J., Weninger, K.R., 1997. Defining the Unknowns of Sonoluminescence, Phys Reports. 281, 65–143.

[6]Johnsen, E., Colonius, T., 2006. Implementation of WENO schemes in compressible multicomponent problems, J. Comput. Phys. 219, 715–732.

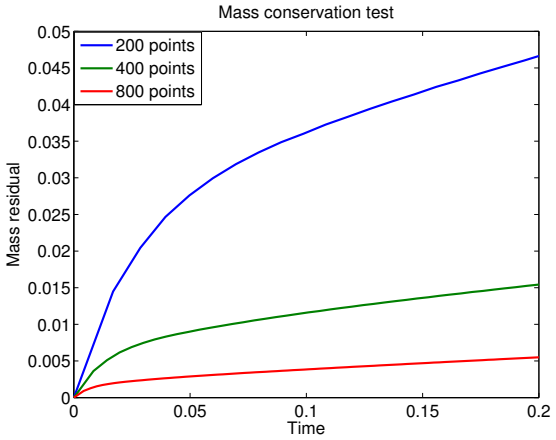

(a) Method One

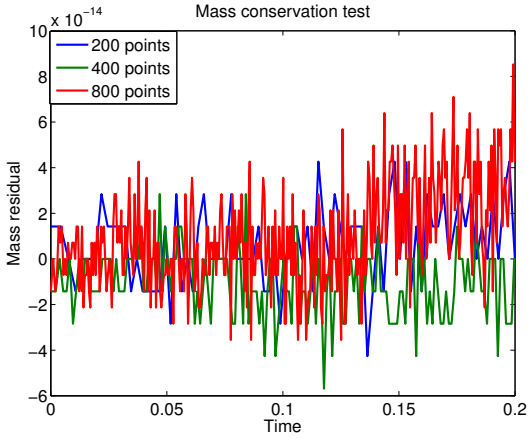

(b) Method Two

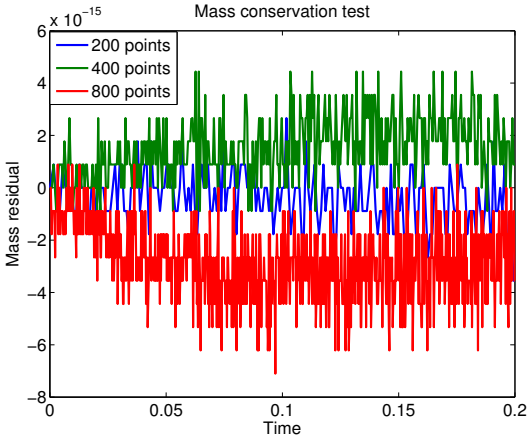

(c) Method Three

Figure 5. Mass residual vs. time for the Sod problem.

[7]Fryxell, B., Olson, K., Ricker, P., Timmes, F.X. , Zingale, M., Lamb, D.Q. ,MacNeice, P., Rosner, R., Truran, J.W., Tufo, H., 2000. FLASH: An Adaptive Mesh Hydrodynamics Code for Modeling Astrophysical Thermonuclear Flashes. Astrophysical Journal, Supplement Series 131 (1) , 273-334

[8]Mohseni, K., and Colonius, T., 2000. Numerical treatment of polar coordinate singularities, J. Comput. Phys. 157, 787–795.

[9]Jiang, G.S., Shu, C.W.,1996. Efficient Implementation of Weighted Eno Schemes, J. Comput. Phys. 72, 78–120.

[10]Johnsen, E., and Colonius, T., 2008. Shock-induced collapse of a gas bubble in shockwave lithotripsy, J. Acoust. Soc. Am. 124, 2011–2020.

[11]Johnsen, E., and Colonius, T., 2009. Numerical simulations of non-spherical bubble collapse, J. Fluid Mech. 629, 231–262.

[12]Sod, G. A., 1978. A survey of several finite difference methods for systems of nonlinear hyperbolic conservation laws, J. Comput. Phys. 27, 1–31.

[13]Li, S.T., 2003. WENO Schemes for Cylindrical and Spherical Geometry, Los Alamos Report LA-UR-03-8922.

[14]Maire, P.H., 2009. A high-order cell-centered Lagrangian scheme for compressible fluid flows in two-dimensional cylindrical geometry, J. Comput. Phys. 228, 6882–6915.

[15]Omang, M., Brve, S., Trulsen, J., 2006. SPH in spherical and cylindrical coordinates, J. Comput. Phys. 212, 391–412.

[16]Sharp, D.H., 1984. An overview of Rayleigh-Taylor Instability. Physica D. 12, 3–18

[17]VonNeumann, J., Richtmyer, R.D., 1950. A Method for the Numerical Calculation of Hydrodynamic Shock. J. Appl. Phys. 21, 232–237

[18]Toro, E. F., 1999. Riemann solvers and numerical methods for fluid dynamics. Heidelberg, Germany: Springer-Verlag.

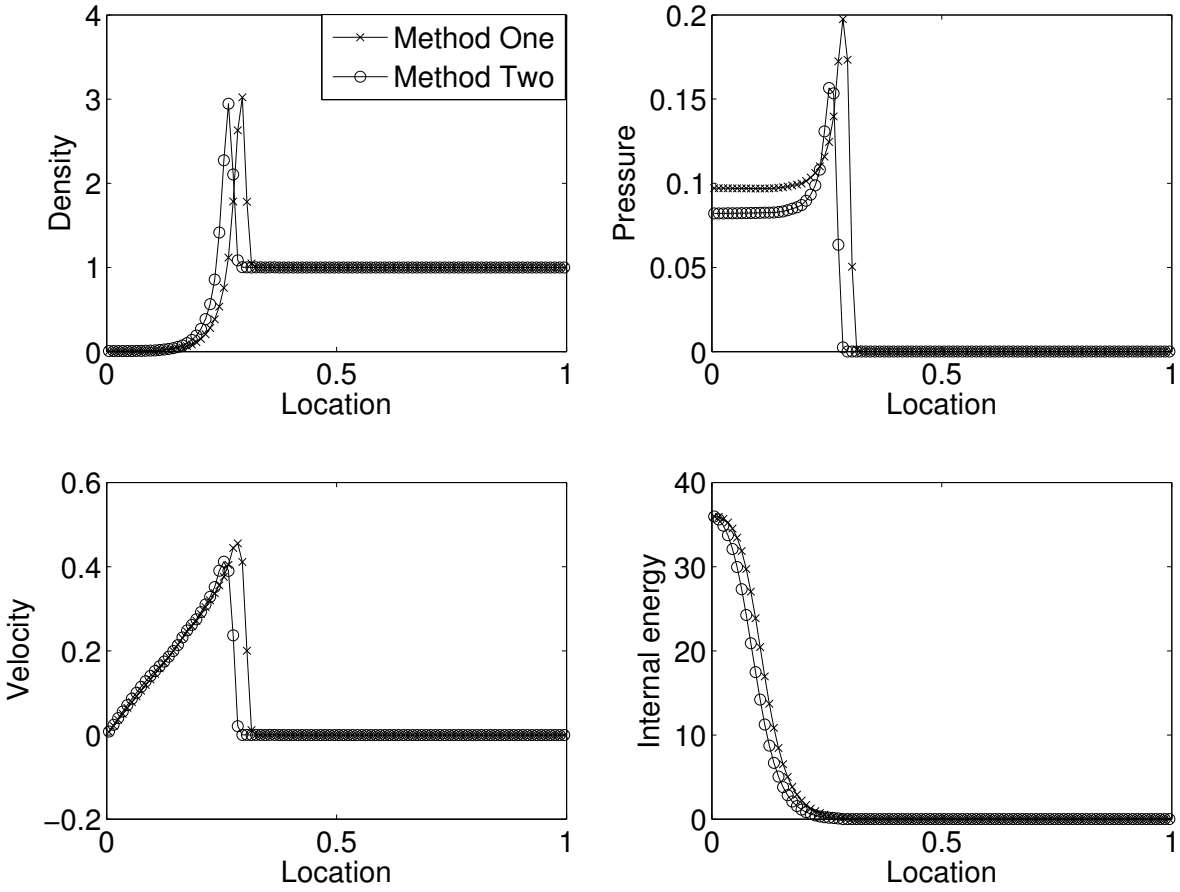

Figure 6. Profiles at $t = 0.2$ for the Sedov problem with 100 points.

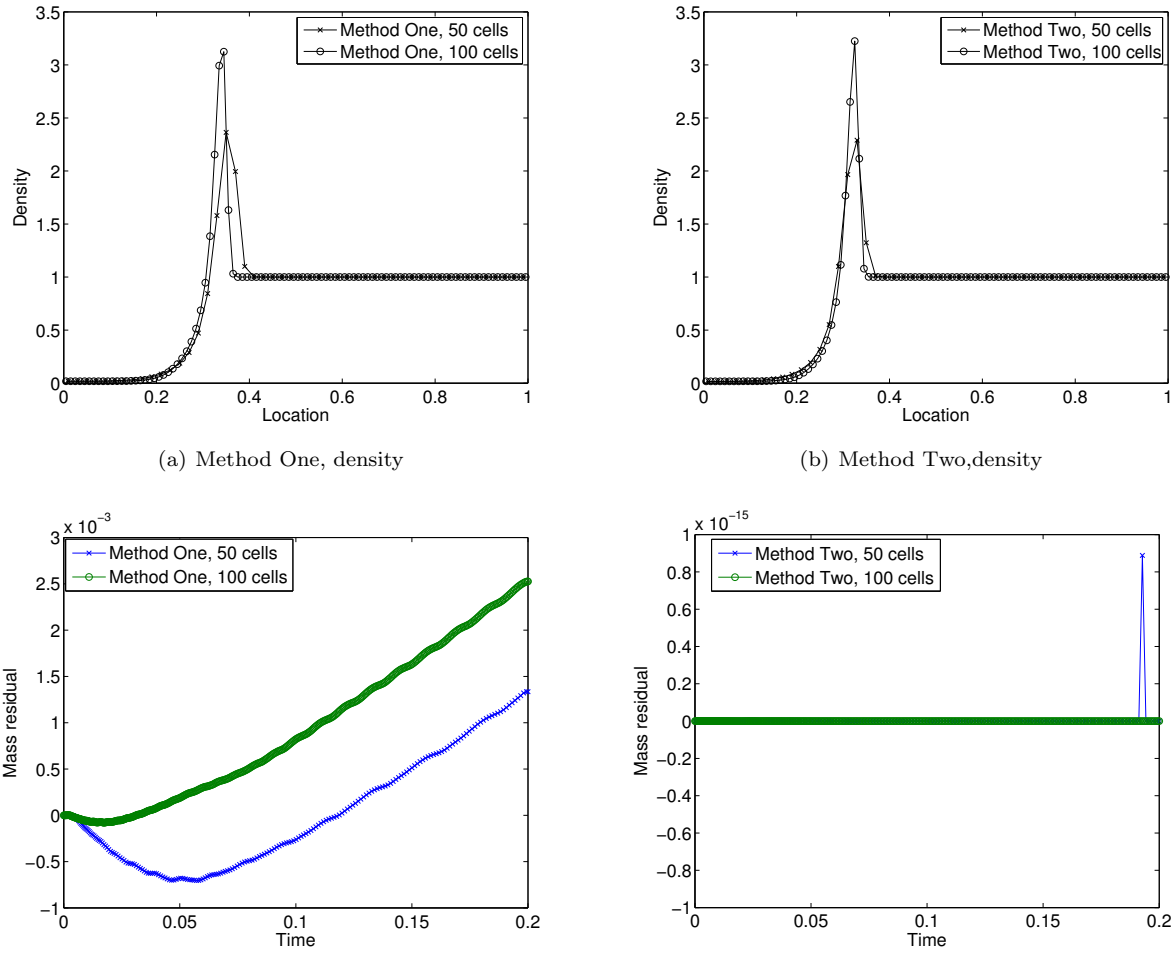

(a) Method One, density

(b) Method Two,density

(c) Method One, mass residual

(d) Method Two,mass residual

Figure 7. The density profile and mass residual for the Sedov blast problem, with different grid size, at t = 0.2